SEMARAK ILMU PUBLISHING

CFD Letters

Journal homepage:
https://semarakilmu.com.my/journals/index.php/CFD_Letters/index
ISSN: 2180-1363

CFD Analysis into the Resistance Estimation of Hard-Chine Monohull using Conventional against Inverted Bows

Ahmad Nasirudin[1], I Ketut Aria Pria Utama[1,*], Sutiyo[2], Andreas Kukuh Priyasambada[1]

[1] Department of Naval Architecture, Faculty of Marine Technology, Institut Teknologi Sepuluh Nopember (ITS), Surabaya 60111, Indonesia
[2] Department of Naval Architecture, Faculty of Engineering and Marine Sciences, Universitas Hang Tuah, Surabaya 60111, Indonesia

ARTICLE INFO

Article history:
Received 10 November 2022
Received in revised form 11 December 2022
Accepted 1 January 2023
Available online 1 June 2023

Keywords:
Resistance; Conventional Bow; Inverted Bow; Hard-Chine Monohull; Computational Fluid Dynamics

ABSTRACT

There are many ways that ship designers can do to get the minimum engine power with the desire ship speed. One of the ways is to design the bow shape with the aim of minimizing ship resistance. In this study, the ship resistance of hard-chine monohull with two different bow shapes that conventional and inverted bows are analyzed. CFD (Computational Fluid Dynamics) approach by using Shear Stress Transport (SST) as turbulence model is used. Different ship speed by Froude numbers Fr 0.2 to 0.7 is applied. The simulation results give convincing evidence that the inverted bow produces lower total resistance compared to the conventional one by about 5% reduction.

1. Introduction

Getting the minimum resistance is one of the important issues in designing a ship. There are many ways that can be done including by optimizing ship hull or choosing different bows. Fitriadhy *et al.,* [1] optimized catamaran hullform to reduce ship total resistance by using CFD technique. Le *et al.,* [2] conducted optimization hullform of container ship by using Neuro-Response Surface Method. Global optimization was applied to optimized trimaran hullform was conducted by Nazemian and Ghadimi [3]. Regarding bow design, Le *et al.,* [4] investigated the effect on ship resistance of blunt and bulbous bow shape by using CFD approach. Utama *et al.,* [5] investigated the effect of the Axe-Bow on the ship resistance reduction of a Trimaran hullform by using experimental and numerical. Sutiyo and Utama [6] analysed the ship resistance characteristics of trimaran vessel with standard NPL 4a hullform and the use of Axe-Bow. The resistance analysis of trimaran vessel with and without Axe-Bow was also conducted by Luhulima *et al.,* [7]. Su *et al.,* [8] studied hydrodynamics performance including resistance of planning trimaran with a Wave-Piercing bow. Besides the bulbous bow, axe-bow, and wave piercing bow there is a bow shape called the inverted or reverse bow. Inverted bow is a bow where the farthest point is not at the top as in conventional one, but rather at below waterline.

* *Corresponding author.*
E-mail address: kutama@na.its.ac.id (I Ketut Aria Pria Utama)

https://doi.org/10.37934/cfdl.15.6.5464

The use of the inverted bow was a common sight on warships in the late 19th century. It helps increase hull efficiency by reducing ship resistance and pitching acceleration. However, in the early 20th century it started to leave since the effect of some drawback such as less reserve buoyancy cause the ship tends to push down under the water and it makes the ship deck extremely wet (since its unflared shape) caused the damage of equipment on the deck. Though it had disappeared, it has begun to come back in the modern era since clearly improving the seakeeping behaviour. Ulstein X-bow and Zumwalt-class destroyer are some of the inverted bow applications examples in the modern era [9].

White *et al.,* [10] investigated the hydrodynamic performance of inverted bow effect on the resistance and seakeeping ability of Navy Combatant planning hull form by using experimental method. Nazemian and Ghadimi optimized inverted bow shapes on a rounded trimaran hull for resistance reduction purpose by using numerical method [11]. In this study, an analysis conducted by comparing the effect of inverted bow especially on resistance of hard-chine monohull at the range of Froude number Fr 0.2 to 0.7. CFD approach of RANS equation base with Shear Stress Transport (SST) as turbulence model are applied.

2. Methodology

2.1 Modelling

A conventional bow hard-chine monohull is taken from Compton [12]. The model length overall is about 2 m, 1.87 m length waterline, 0.36 m width, 0.32 m height, 0.119 m draught, 35.9 kg displacement, and 0.468 block coefficient. The conventional bow hullform then modified become inverted one by adding about 20% of Length overall at the bow. The conventional and inverted bow hullform can be seen in Figure 1, while the particulars shown in Table 1:

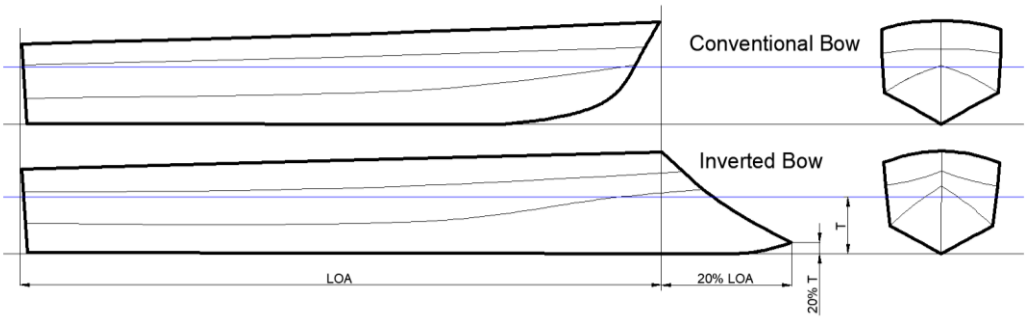

Fig. 1. Conventional and inverted bow

Table 1
Conventional and Inverted bow particulars

Particulars	Conventional bow	Inverted bow
LOA	2.00 m	2.41 m
LWL	1.87 m	2.26 m
B	0.36 m	0.36 m
H	0.32 m	0.32 m
T	0.119 m	0.115 m
Cb	0.468	0.387
Displacement (□)	35.9 kg (352.2 N)	35.15 kg (344.8 N)
Wetted Surface Area (S)	0.71 m^2	0.83 m^2
Difference Displacement	-	-2.13 %

2.2 Resistance Representation

The ship resistance is analyzed at Froude numbers Fr 0.2 to 0.7 in 0.1 increment. The resistance comparison results of conventional and inverted bow are presented by total resistance, friction resistance, and residuary resistance. The friction resistance is obtained by taking friction resistance coefficient (C_F) from ITTC-1957 correlation line as shown in Eq. (1).

$$C_F = \frac{0.075}{(\log_{10} R_e - 2)^2} \tag{1}$$

where R_e is Reynolds number.

2.3 Numerical Investigation

Numerical investigation is carried out by using commercial computational fluid dynamics software ANSYS CFX program which has been used in solving fluid dynamic problems in marine vehicles application by several authors [13-15]. The several stages are conducted in this investigation including boundary condition, grid generation, and V&V study.

2.3.1 Governing equations

In the computational fluid dynamics (CFD) model, the Reynolds-averaged Navier-Stokes (RANS) approach is a three-dimensional equation that was created and employed. The ANSYS-CFX programme was built to solve flow issues in the walls of ships, and one of the equations that it generated to do so was constant viscous incompressible flow. It is possible to express the averaged continuity and momentum equations for incompressible flows using the two equations [16]. The equations of mass and momentum can be written as follows in Eqs. (2) and (3):

$$\frac{\partial \rho}{\partial t} + \nabla.(\rho U) = 0 \tag{2}$$

$$\frac{\partial (\rho U)}{\partial t} + \nabla.(\rho U\ x\ U) = -\nabla p + \nabla.\tau + S_M \tag{3}$$

where the stress tensor, τ is related to the strain rate.

The governing equation of CFD for total energy is presented in the Eq. (4):

$$\frac{\partial (\rho h_{tot})}{\partial t} - \frac{\partial p}{\partial t} + \nabla.(\rho U h_{tot}) = \nabla(\lambda \nabla T) + \nabla(U.\tau) + U.S_M + S_E \tag{4}$$

where h_{tot} is the total enthalpy

The term $+\nabla(U.\tau)$ represents the work due to viscous stresses and is called the viscous work term. The term $U.S_M$ represents the work due to external momentum sources and is currently neglected.

Furthermore, Reynolds Averaged Navier-Stokes (RANS) was developed, which is a modification of steady Navier-Stokes that includes averaged and fluctuating variables. Anderson classifies the

RANS equation-based turbulence model as a statistical turbulence model due to the statistical averaging approach utilised to derive the equation [17].

The SST model is able to obtain an appropriate model formulation for a wide variety of applications since it combines the benefits of the k-ω model with other relevant factors. In order to do this, a blending function known as F1 is added. This function has a value of one in the region immediately next to the solid surface, while it has a value of zero in the flow domain farther away from the wall. The k-ω wall area and the k-ε model for the remainder of the flow are both activated as a result of this. With this method, the desirable near-wall performance of the k-ω model may be used without the risk of making inaccuracies due to the model's sensitivity to free stream conditions. The modelled equations for the turbulent kinetic energy k and the turbulence frequency ω are as follows:

$$\frac{\partial(\rho k)}{\partial t}+\frac{\partial(\partial u_j k)}{\partial x_j}=P-\beta^*\rho\omega k+\frac{\partial}{\partial x_j}\left[(\mu+\sigma_k\mu_t)\frac{\partial k}{\partial x_j}\right] \tag{5}$$

$$\frac{\partial(\rho\omega)}{\partial t}+\frac{\partial(\rho u_j\omega)}{\partial x_j}=\frac{\gamma}{v_t}P-\beta\rho\omega^2+\frac{\partial}{\partial x_j}\left[(\mu+\sigma_\omega\mu_t)\frac{\partial\omega}{\partial x_j}\right]+2(1-F_1)2\rho\sigma_{\omega 2}\frac{1}{\omega}\frac{\partial k}{\partial x_j}\frac{\partial\omega}{\partial x_j} \tag{6}$$

Its performance has been reported by Menter and Esch [18]. In a recent NASA Technical Memorandum by Bardina *et al.,* the SST model was rated the most accurate model in its class [19].

2.3.2 Boundary condition

Figure 2 details the domain size and boundary conditions. The following boundary criteria are listed: The top, side, and bottom walls are subject to the free-slip condition, while the wall plane is applicable to the symmetry condition.

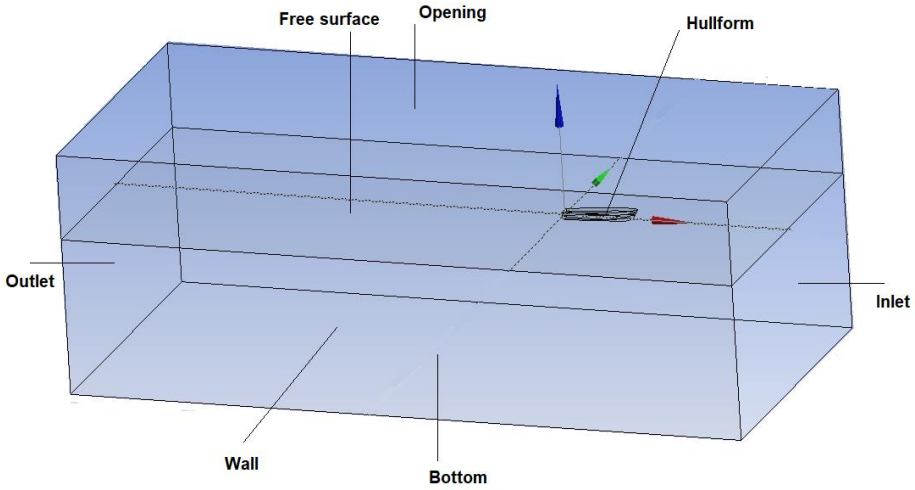

Fig. 2. Boundary conditions

The flow velocity at the inlet is defined as the studied speed, while the static pressure defined as a function of water-level height is applied at the outlet. Additionally, the common set of the free surface is specified by identifying the volume-fraction function of water and an equation for the initial water level height.

2.3.3 Grid generation

In this particular investigation, the production of the mesh was carried out via Design Modeler. In order to discretize the computation domain, both structured and unstructured meshes were utilized. In consideration of the intricate geometrical features of the hull, a mesh consisting of triangle elements is constructed on the surface of the hull, and the boundary layer is then refined with prism elements by expanding the surface mesh node. In the vicinity of the boat, tetrahedral components are inflated to fill the space, while in the distant field, an unstructured mesh with modelling is produced to cut down on the total number of elements, as shown in Figure 3.

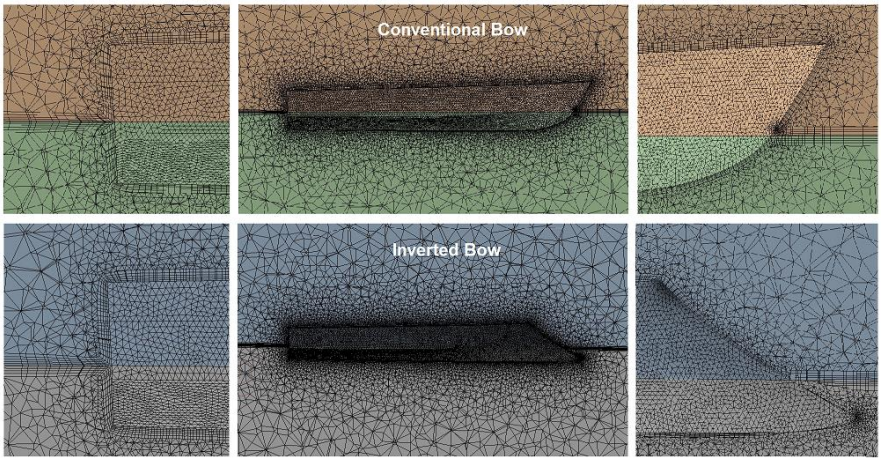

Fig. 3. Unstructured mesh with inflation

In this particular investigation the production of the mesh was carried out It is crucial to the computation process that the mesh size be appropriately chosen Due to the high number of elements a fine mesh may reliably provide believable results in ANSYS CFX but it also significantly increases the computational cost and time consumption Consequently mesh convergence studies are performed at a Froude number of 0 2 for the standard bow hull shape to estimate the mesh size with adequate numerical precision and element number Table 2 and Figure 4 from Chung's grid independence analysis [20].

Table 2
Grid independence study

Bow type	Total element	Total Resist. Coeff. (C_T)	Difference (%)
Conventional Bow	80,569	0.0197	-
	170,654	0.0157	25.5
	365,564	0.0141	11.1
	750,625	0.0122	16.3
	1,402,364	0.0113	7.3
	3,136,568	0.0111	1.7
Inverted Bow	75,645	0.0168	-
	155,665	0.0139	20.9
	324,652	0.0105	33.1
	670,625	0.0089	17.2
	1,220,364	0.0080	12.2
	2,865,232	0.0078	1.9

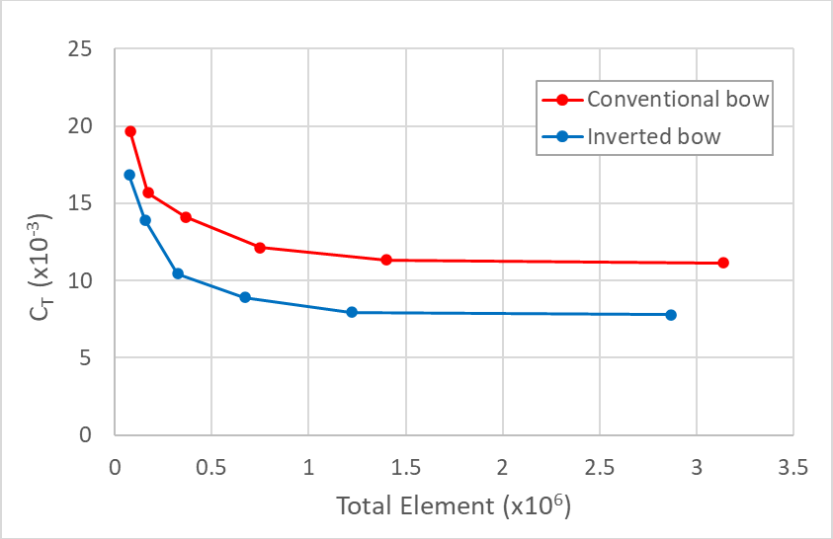

Fig. 4. Grid Independence

2.3.4 V&V study of total resistance

Convergence studies of parameters are performed following a systematic refinement process to create multiple solutions. The numerical uncertainty of the CFD model utilizes the data in Table 2. In this paper, Richardson's extrapolation method for grid convergence could be a proper choice for estimating the mesh error [21]. The grid convergence study was conducted based on the ITTC uncertainty analysis recommendation [22]. The convergence ratio RG can be written as:

$$R_G = \frac{\varepsilon_{21}}{\varepsilon_{32}} \tag{7}$$

where ε_{21} is different of estimation where is ratio of number of element medium to fine and ε_{32} is different of estimation where is ratio of number of elements fine to coarse.

Convergence conditions of this system must first be clarified to assess the extrapolated value from the equations above. The convergence conditions are as follows:

i. Monotonic convergence: 0 < Ri < 1
ii. Oscillatory convergence: Ri < 1
iii. Divergence: Ri > 1

For monotonic convergence, a generalized Richardson extrapolation is applied to estimate the errors and uncertainties. For oscillatory convergence, the results exhibit some oscillations. Lastly, for divergence, the results diverge, while errors and uncertainties are impossible to determine.

The grid convergence index (GCI) is a standardized way to report grid-convergence quality. It is calculated at refinement steps. Thus, we calculated a GCI for steps from grids 3 to 2, and from 2 to 1, where e is the error between the two grids and Fs is the safety factor (Fs=1.25).

The investigation on convergence was carried out using three distinct mesh resolutions, which were labelled as "coarse," "medium," and "fine," respectively. The mesh was modified by changing the face size while maintaining the body size with a fixed element size. This was done in order to get the desired effect. Due to the fact that the mesh resolution was determined by the usual wall calculation, the inflation layer remained constant for the whole of the investigation, as shown in Table 3.

Table 3
Three varying mesh resolution details

Bow type	Detail	Fine (1)	Medium (2)	Coarse (3)
Conventional bow	Body sizing (m)	0.25	0.3	0.5
	Face sizing (m)	0.015	0.025	0.04
	Number of Elements (NE)	2,865,232	1,220,364	670,625
	Drag coefficient (C_T)	0.0110	0.0112	0.0125
Inverted bow	Body sizing (m)	0.25	0.3	0.5
	Face sizing (m)	0.015	0.025	0.04
	Number of Elements (NE)	3,136568	1,402,364	750,625
	Drag coefficient (C_T)	0.0111	0.0113	0.0122

The process is the same for time or any other study parameter. As for the refinement ratio r_i, the recommended value is 1.424, since the value is large enough to be sensitive to parameter changes and small enough to generate at least three successive solutions maintaining. A larger refinement ratio may be used; however, the mesh value must be at least three. Based on formulas in the used equation section, outcomes have been calculated and presented at Table 4.

Table 4
The uncertainty analysis

Outcome	Equation	Conventional bow	Inverted Bow
Difference of estimation	$\varepsilon_{21}=NE_2/NE_1$	2.2366	2.3479
	$\varepsilon_{32}= NE_3/NE_2$	1.8683	1.8197
Refinement ratio	$r_{21}=C_{T2} -C_{T1}$	0.0002	0.0008
	$r_{32} = C_{T3} -C_{T2}$	0.0008	0.0014
Convergence	$R_i=\varepsilon_{21}/\varepsilon_{32}$	0.2321	0.6018
Order of accuracy	$p=\ln(\varepsilon_{21}/\varepsilon_{32})/\ln(r_i)$	1.8146	0.5949
Extrapolated relative error	$e_{21=} \varepsilon_{21}/r_i^p-1$	0.0000	0.0002
	$e_{32}= \varepsilon_{32}/r_i^p-1$	0.0003	0.0006
Grid convergence index (GCI)	$GCI_{21}=Fs\|e_{21}\|$	0.0000	0.0003
	$GCI_{32=} Fs\|e_{32}\|$	0.0049	0.0510

The mesh converged with varied fineness's of mesh, as shown by the graphs, which showed that the drag coefficient converged. In spite of this, the tiny mesh was selected for the inquiry since it offers a better level of precision to the simulation and, as a result, reduces the amount of error that is introduced throughout the investigation.

3. Result and Discussion

The resistance results for conventional and inverted bow hullform are presented. Table 5 and Figures 5 (a) to (c) show the total resistance, friction resistance, and residuary resistance of both bows respectively with the function of ship speeds which is expressed by the Froude number Fr. The differences of each resistance of inverted to conventional bow are also presented. For residuary resistance (Table 5 and Figure 5 (c)), the inverted bow produces lower resistance than conventional one by an average of about 10.4% difference. This result is also in line with the study reported by White *et al.,* [10]. However, for friction resistance (Table 5 and Figure 5(b)), the inverted bow produces higher resistance than conventional one of about 45.4%. This can be explained that because the wetted surface area of inverted bow is larger than conventional one. For total resistance (Table 5 and Figure 5 (a)), for all ship speed conditions, it is clearly shown that the total resistance produced

by inverted bow is lower than conventional one by an average difference of about 5%. This means that the inverted bow has better performance in saving the engine power than the conventional one.

Table 5
Total Resistance, friction resistance, and residuary resistance

Fr	Total Resistance (R_T)			Friction Resistance (R_F)			Residuary Resistance (R_R)		
	Conv (N)	Inv (N)	Diff (%)	Conv (N)	Inv (N)	Diff (%)	Conv (N)	Inv (N)	Diff (%)
0.2	3.04	3.00	-1.3%	0.34	0.49	45.2%	2.70	2.51	-7.1%
0.3	9.64	8.24	-14.5%	0.79	1.15	45.3%	8.85	7.09	-19.8%
0.4	18.28	17.37	-5.0%	1.45	2.11	45.4%	16.83	15.26	-9.3%
0.5	27.32	27.11	-0.8%	2.33	3.39	45.4%	24.99	23.72	-5.1%
0.6	32.22	31.18	-3.3%	3.43	4.99	45.5%	28.80	26.19	-9.1%
0.7	39.27	37.25	-5.2%	4.75	6.92	45.5%	34.52	30.33	-12.1%
avg	-	-	-5.0%	-	-	45.4%	-	-	-10.4%

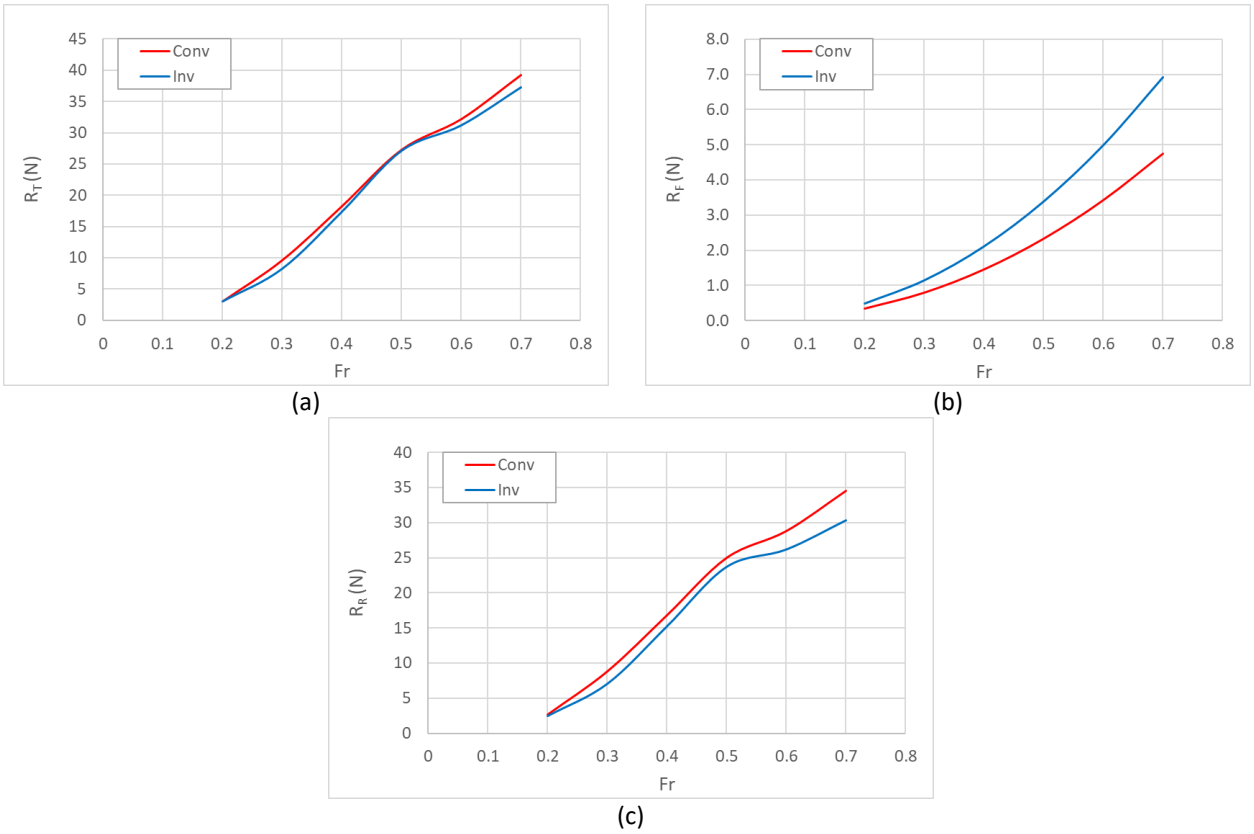

Fig. 5. Resistance comparison of conventional and inverted bow (a) Total Resistance (b) Friction Resistance (c) Residuary Resistance

The reason why the inverted bow produces less resistance than the conventional one can be explained in Figure 6 (a) and (b). Figure 6 (a) presents the wave profiles around the hull at Froude number 0.2, 0.4, and 0.6, while Figure 6 (b) is for Froude number 0.3, 0.5, and 0.7. In those figures x-axis is wave propagation along hullform and y-axis is wave height. From all wave profiles, there are shown that the wave heights produced by inverted bow are lower than conventional one for all ship speed conditions. This is also proven by the wave contour of several ship speed condition which can be seen in Figure 7. Figures 7 (a) to (d) present the wave contour comparison of conventional (above part) and inverted bow (below part) at Froude number 0.4, 0.5, 0.6, and 0.7 respectively.

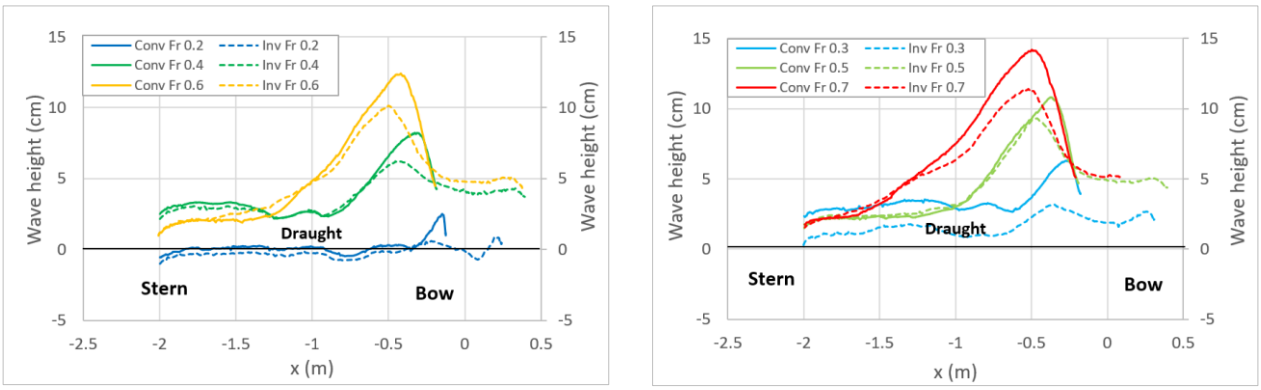

(a) (b)

Fig. 6. Wave profile comparison of conventional and inverted bow hullform at different Froude number (a) Fr 0.2, 0.4, and 0.6 (b) Fr 0.3, 0.5, and 0.7

Figure 7 (a) shows visually that for inverted bow hullform at Fr 0.4 produces lower wave crest than conventional one. This can be confirmed by the wave profile in figure 6(a) that the wave crest height of inverted bow is about 6 cm, while conventional bow produces about 8 cm wave height measure from draught waterline. Likewise for Fr 0.5 to 0.7 as seen in Figure 7(b) to (d) that inverted bows produce lower wave than conventional one. These results can be confirmed by the wave profile in Figure 6 that for Fr 0.5, 0.6, and 0.7, the wave crests height of inverted bow is about 9 cm, 10 cm, and 11 cm, while conventional bow produces about 11 cm, 12 cm, and 14 cm respectively.

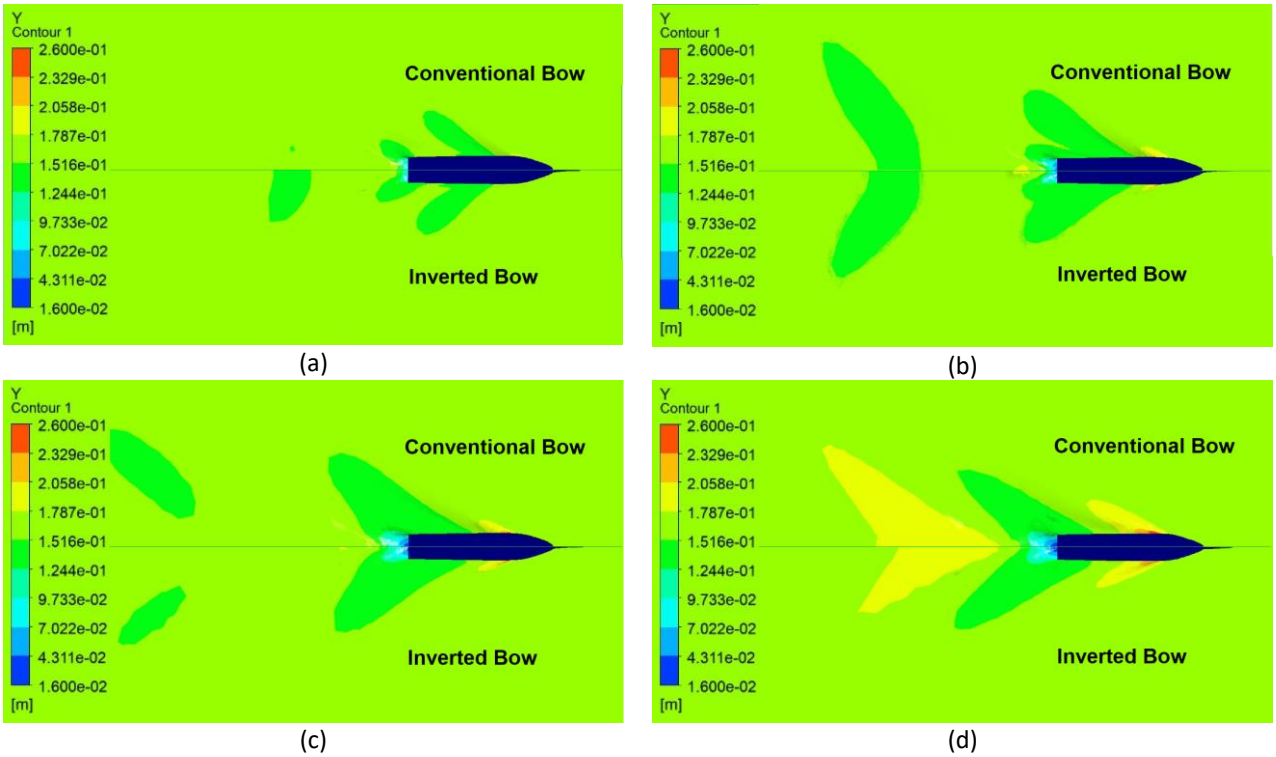

(a) (b)

(c) (d)

Fig. 7. Wave contour comparison of conventional and inverted bow hullform (a) Froude number 0.4 (b) Froude number 0.5 (c) Froude number 0.6 (d) Froude number 0.7

The factor that affects the wave height produced by the ship is the pressure around the hullform. Figures 8 (a) to (d) show the comparison of pressure around the bow of conventional and inverted shape at Fr 0.4, 0.5, 0.6, and 0.7 respectively. Based on those figures, the pressures around the bow produced by inverted shape are relatively small (tend to be flat), while the conventional one tends

to be high. This is due to the positive flare of the conventional bow where the entrance angle of the bow increasing upwards, so that the pressure in the bow becomes large and produces a large bow wave. Whereas, for the inverted one, the entrance angle is getting smaller upwards. This makes the pressure in the bow to be low which produces a small bow wave.

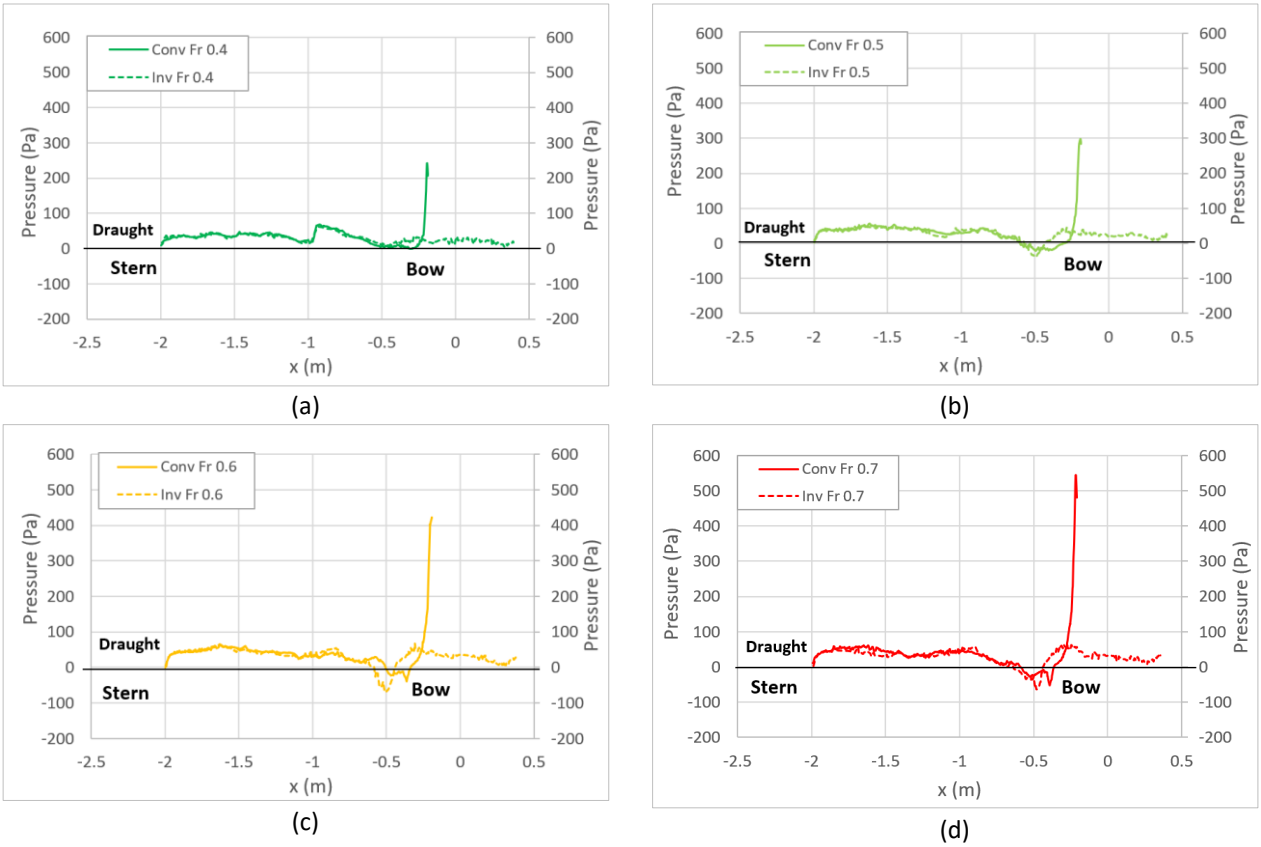

Fig. 8. Wave profile and pressure around the hull (a) Fr 0.6 (b) Fr 0.7

4. Conclusions

A resistance analysis into the conventional and inverted bow on hard-chine monohull by using CFD approach with RANS equation and Shear Stress Transport (SST) turbulence model has been presented successfully. The result shows that the inverted bow hullform provided lower total resistance than the conventional one at every ship speed condition. The average total resistance reduction of inverted bow is about 5% from the conventional one. This is proven by the wave height generated that at Fr 0.4, 0.5, 0.6, and 0.7, the wave crests height of inverted bow is about 6 cm, 9 cm, 10 cm, and 11 cm, while conventional bow produces about 8 cm, 11 cm, 12 cm, and 14 cm respectively.

Acknowledgement

The authors wish to thank the Directorate of Research and Community Services (DRPM), Institut Teknologi Sepuluh Nopember (ITS), for financing the research under the project scheme of the Publication Writing and IPR Incentive Program (PPHKI) Number 668/IT2/T/HK.00.01/2022.

References

[1] Fitriadhy, Ahmad, Nurul Shukna Rizat, Atiyah Raihanah Abd Razak, Sheikh Fakhruradzi Abdullah, Faisal Mahmuddin, and Alamsyah Kurniawan. "Optimization Modelling of a Catamaran Hull Form towards Reducing Ship's Total Resistance." *CFD Letters* 14, no. 4 (2022): 67-79. https://doi.org/10.37934/cfdl.14.4.6779

[2] Lee, Soon-Sub, Jae-Chul Lee, Sung-Chul Shin, Soo-Young Kim, and Hyun-Sik Yoon. "A study on optimization of ship hull form based on neuro-response surface method (NRSM)." *Journal of Marine Science and Technology* 22, no. 6 (2014): 12.

[3] Nazemian, Amin, and Parviz Ghadimi. "Global optimization of trimaran hull form to get minimum resistance by slender body method." *Journal of the Brazilian Society of Mechanical Sciences and Engineering* 43 (2021): 1-20. https://doi.org/10.1007/s40430-020-02791-8

[4] Le, Trung-Kien, Ngo Van He, Ngo Van Hien, and Ngoc-Tam Bui. "Effects of a bulbous bow shape on added resistance acting on the hull of a ship in regular head wave." *Journal of Marine Science and Engineering* 9, no. 6 (2021): 559. https://doi.org/10.3390/jmse9060559

[5] Utama, I. K. A. P., and I. K. Suastika. "Experimental and Numerical Investigation into the Effect of the Axe-Bow on the Drag Reduction of a Trimaran Configuration." *International Journal of Technology* 12, no. 3 (2021): 527-538. https://doi.org/10.14716/ijtech.v12i3.4659

[6] Utama, I. Ketut Aria Pria. "CFD Analysis into the Drag Characteristics of Trimaran Vessel: Comparative Study between Standard NPL 4a and the use of Axe-Bow." In *IOP Conference Series: Earth and Environmental Science*, vol. 799, no. 1, p. 012007. IOP Publishing, 2021. https://doi.org/10.1088/1755-1315/799/1/012007

[7] Luhulima, Richard Benny, Sutiyo Sutiyo, and I. Pria Utama. "The Resistance and EEDI Analysis of Trimaran Vessel with and without Axe-bow." *NAŠE MORE: znanstveni časopis za more i pomorstvo* 69, no. 3 (2022): 0-0. https://doi.org/10.17818/NM/2022/3.1

[8] Su, Guangsheng, Hailong Shen, and Yumin Su. "Numerical prediction of hydrodynamic performance of planing trimaran with a wave-piercing bow." *Journal of Marine Science and Engineering* 8, no. 11 (2020): 897. https://doi.org/10.3390/jmse8110897

[9] Philippe Goubault, Stephane Le Pallec, and Yann Floch. "Why Consider Inverted Bows on Militay Ships? Or why Not?." *Association Technique Maritime et Aéronautique* (*ATMA) 2018,* no. 2729 (2018).

[10] White, Jeffrey K., Stefano Brizzolara, and William Beaver. "Effect of Inverted Bow on the Hydrodynamic Performance of Navy Combatant Hull Forms." In *SNAME Maritime Convention and 5th World Maritime Technology Conference*. OnePetro, 2015. https://doi.org/10.5957/WMTC-2015-038

[11] Nazemian, A., and P. Ghadimi. "Automated CFD-based optimization of inverted bow shape of a trimaran ship: An applicable and efficient optimization platform." *Scientia Iranica* 28, no. 5 B (2021): 2751-2768.

[12] Compton, Roger H. "Resistance of a systematic series of semiplaning transom-stern hulls." *Marine Technology and SNAME News* 23, no. 04 (1986): 345-370. https://doi.org/10.5957/mt1.1986.23.4.345

[13] Jabar, Siti Norbakyah, and Salisa Abdul Rahman. "A Comparative Study on Components Sizing for Conventional Boat and Pherb Powertrains using Water Driving Cycle." *Journal of Advanced Research in Applied Sciences and Engineering Technology* 16, no. 1 (2019): 41-48.

[14] Waskito, Kurniawan Teguh. "On the High-Performance Hydrodynamics Design of a Trimaran Fishing Vessel." *Journal of Advanced Research in Fluid Mechanics and Thermal Sciences* 83, no. 1 (2021): 17-33. https://doi.org/10.37934/arfmts.83.1.1733

[15] Utomo, Allessandro Setyo Anggito. "Comparison of Drag Reduction Effect on Barge Model Ship Using Ultrafine Bubble and Microbubble Injection." *Journal of Advanced Research in Fluid Mechanics and Thermal Sciences* 96, no. 2 (2022): 134-143. https://doi.org/10.37934/arfmts.96.2.134143

[16] Ansys, C. "Ansys Cfx-Solver Modeling Guide. Canonsburg, PA, USA: ANSYS." (2020).

[17] Anderson, John David, and John Wendt. *Computational fluid dynamics*. Vol. 206. New York: McGraw-Hill, 1995.

[18] Menter, Florian R. "Elements of Inductrial Heat Tranfer Predictions." In *16th Brazilian Congress of Mechanical Engineering (COBEM), Uberlandia, Brazil, 2001*. 2001.

[19] Bardina, Jorge E., Peter G. Huang, and Thomas J. Coakley. *Turbulence modeling validation, testing, and development*. No. A-976276. 1997. https://doi.org/10.2514/6.1997-2121

[20] Chung, T. J. *Computational fluid dynamics*. Cambridge university press, 2002. https://doi.org/10.1017/CBO9780511606205

[21] Zingg, D. "Viscous airfoil computations using Richardson extrapolation." In *10th Computational Fluid Dynamics Conference*, p. 1559. 1991. https://doi.org/10.2514/6.1991-1559

[22] ITTC. "CFD Verification." *ITTC – Recommendation Procedure Guideline*. (1999): 485–487.